Novel Mixed-Mode Phase Transition Involving a Composition-Dependent Displacive Component

S. Nag, A. Devaraj, R. Srinivasan, R. E. A. Williams, N. Gupta, G. B. Viswanathan, J. S. Tiley, S. Banerjee, S. G. Srinivasan, H. L. Fraser, and R. Banerjee

Phys. Rev. Lett. **106**, 245701 — Published 17 June 2011

DOI: 10.1103/PhysRevLett.106.245701

Novel mixed-mode phase transition involving a composition-dependent displacive component

S. Nag[1], A. Devaraj[1], R. Srinivasan[2], R. E. A. Williams[3], N. Gupta[1], G. B. Viswanathan[4], J. S. Tiley[4], S. Banerjee[5], S. G. Srinivasan[1*], H. L. Fraser[3], and R. Banerjee[1†]

[1] *Department of Materials Science and Engineering, University of North Texas, Denton, USA*
[2] *ExxonMobil Research and Engineering Company, Annandale, USA*
[3] *Department of Materials Science and Engineering, The Ohio State University, Columbus, USA*
[4] *Materials and Manufacturing Directorate, Air Force Research Laboratory, Dayton, USA, and*
[5] *Department of Atomic Energy and Atomic Energy Commission, Mumbai, India.*

Solid-solid displacive, structural phase transformations typically undergo a discrete structural change from the parent to the product phase. Coupling electron microscopy, three-dimensional atom probe, and first-principles computations, we present the first direct evidence of a novel mechanism for a coupled diffusional-displacive transformation in an important class of titanium-molybdenum alloys wherein the displacive component in the product phase changes continuously, as a function of its composition. These results cannot be explained by conventional theories and have wide implications for numerous other solid-solid transformations.

Solid-solid phase transformations are ubiquitous in nature and fundamental to modern materials science. The so-called first-order transformations involve discrete nucleation and growth of the product phase in the parent phase matrix, while second (or higher) order ones involve a homogeneous continuous transformation from the parent to the product phases. Importantly, classical nucleation theory of first-order transformations assume that the second phase nucleus has the equilibrium composition and crystal structure of the product phase. The first-order transformations are further classified as diffusional, displacive, and coupled diffusional-displacive (mixed-mode) depending on the operative transformation mechanism. Mixed-mode transformations, such as the classical bainite transformation in steels, typically include coupled diffusional and displacive (often shear or shuffle-based) components. The Bainite transformation in the Fe-C system involves decomposition of a face-centered cubic (fcc) parent phase (γ) into a body-centered cubic (bcc) α and orthorhombic cementite (Fe_3C) phases via diffusive partitioning of carbon followed by a displacive change in crystal structure. Importantly, this γ to α and similar first-order transformations, are believed to involve a single discrete step over an activation energy barrier. This letter, for the first time, presents evidence for a new mixed-mode solid-solid transformation wherein both a diffusive compositional change and a displacive structural change occur in a coupled yet continuous fashion, thus displaying features of a continuous solid-solid transformation while still being a first order transformation. The newly discovered features include a partially collapsed intermediate structure lying in between parent and product phases, and composition dependent displacive component of transformation (i.e. extent of collapse within the embryos). Our proposed mechanism explains the observed partially transformed embryos, lying in between the two end states, with local minima in the free energy landscape of the system.

This new transformation mechanism has been observed for the bcc (β) to the hexagonal ω phase transformation, directly relevant to a wide variety of important engineering alloys involving Group IV elements. At ambient pressure, titanium (Ti), zirconium (Zr), hafnium (Hf), and other Group IV elements exhibit two distinct allotriomorphs – stable low temperature hexagonal close-packed (hcp) α and stable higher temperature bcc β phases. Alloys of these elements, containing a critical concentration of β-stabilizing elements, form a metastable, non-close packed hexagonal ω phase upon rapidly cooling from the high temperature single β phase field followed by isothermal annealing [1]. The ω phase has been actively studied for over 50-years due to its complex formation mechanism and its influence on mechanical and superconducting properties [2–5]. It is now widely accepted that athermal ω precipitates retain the composition of the parent β matrix, and have been postulated to form by a purely displacive collapse of the {111} planes of the bcc phase via a shuffle mechanism [6, 7]. In contrast, the isothermal ω precipitates have been postulated to form via a thermally-activated process involving diffusion-based compositional partitioning followed by the collapse of {111} bcc planes in the compositionally-depleted regions [6, 7].

In this letter, we present the salient aspects of the newly proposed transformation mechanism using titanium-molybdenum (Ti-Mo) alloys as a model system. Experiments reveal concurrent compositional and structural instabilities within the undercooled bcc β phase of a Ti-Mo alloy leading to the formation of embryos with partially transformed ω-like structures. Nanometer-scale molybdenum-depleted pockets, arising from the early stages of phase separation (clustering) within the β matrix, have been qualitatively detected using aberration-corrected high-resolution scanning transmission electron microscopy (HRSTEM) and quantitatively measured

†Email: banerjee@unt.edu
*Email: srinivasan.srivilliputhur@unt.edu

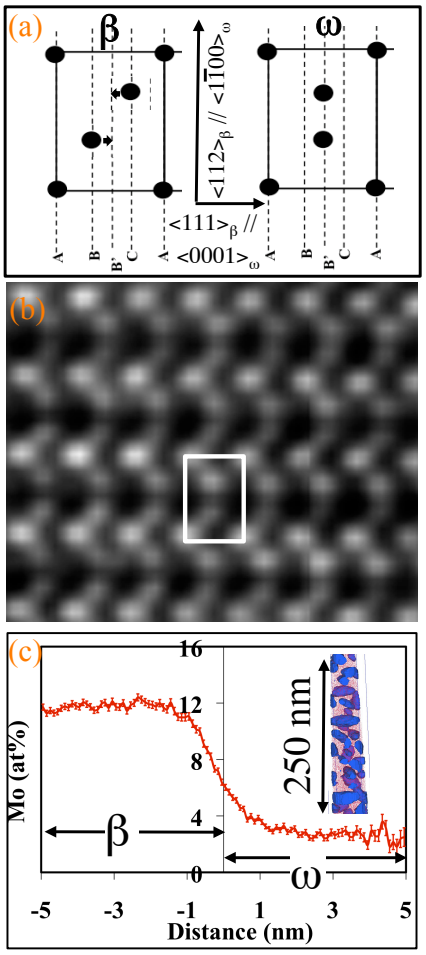

FIG. 1: (a) Schematic arrangement of atoms as seen from $< 110 > \beta$ zone axis, along with the β and fully collapsed ω motifs in a 748K/30 minutes aged Ti-9at%Mo sample. Small arrows show the shifts of atoms along $< 111 > \beta$ directions. (b) HRTEM image recorded along $< 011 > \beta$ zone axis showing the collapse in atomic columns corresponding to well developed ω phase. (c) Proximity histogram using Ti=93 at% isosurface that shows substantial compositional partitioning between the β and ω phases. Inset shows the corresponding 3DAP reconstruction exhibiting the Ti-rich regions.

by three-dimensional atom probe (3DAP). Concurrent structural instabilities cause partial collapse of $\{111\}_\beta$ planes within these Mo-depleted pockets, leading to the formation of embryonic ω-like structures directly imaged at atomic resolution using HRSTEM. Finally, first-principles electronic-structure calculations reveal that these partially transformed ω-like structures correspond to local energy minima in the free energy landscape, are composition-dependent, and lie between parent β and fully transformed ω phases.

Samples of forged and annealed Ti-9at%Mo (18wt% Mo) alloy from the TIMETAL^{TM} company, were solution heat-treated in the single β phase field at 1273K for 30 minutes in a vacuum furnace ($\sim$1 x 10^{-6} torr) and then rapidly cooled at $\sim$ 10°C/sec in Ar gas. Some of these rapidly cooled samples were subsequently annealed

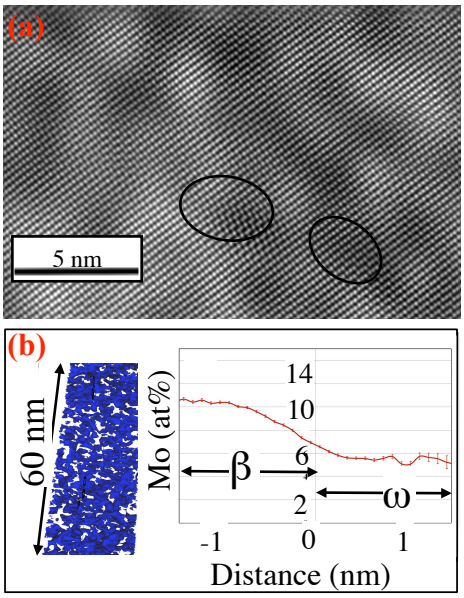

FIG. 2: (a) Filtered HAADF-HRSTEM image of rapidly cooled Ti-9at%Mo sample recorded along $< 011 > \beta$ zone axis showing the atomic columns within the bcc matrix as well as marked regions corresponding to the ω embryos. (b) 3DAP atomic reconstruction of Ti-rich regions as iso-concentration surfaces (Ti = 93 at%). Corresponding proximity histogram shows the compositions of solute-rich and solute-lean regions.

at 748K for 30 minutes. Microscopy specimens were prepared using the FEI Nova Nanolab 200 dual-beam Focused Ion Beam (FIB) system, and characterized using a FEI Titan 80-300 TEM and in a local electrode atom probe (LEAP^{TM}) system from Cameca Instruments Inc [8]. The LEAP samples were run in electric-field evaporation mode at 70K, with an evaporation rate of 0.2–1.0 % and a voltage pulse fraction at 20% of the steady-state applied voltage. TEM studies of atomic resolution Z-contrast imaging (through High Angle Annular Dark Field (HAADF)-HRSTEM) was performed at 300 kV using a CEOS probe aberration corrector.

Well-developed 30–50 nm sized ω precipitates (not shown) have been observed in the Ti-9at%Mo sample that was β solutionized (at 1273K), quenched, and then isothermally annealed for 30 mins at 748K. The displacement of atomic columns within the bcc phase, equivalent to the collapse of the $\{111\}\beta$ planes, leading to the formation of ω phase is illustrated by the schematic β-motif in Fig.1a, and has been discussed in the literature [1, 6, 7]. This fully developed ω structure is clearly visible in the atomic-resolution TEM image shown in Fig. 1(b) from the 748K annealed Ti-9at%Mo sample. The same sample has also been analyzed using 3D atom probe and a tomographic reconstruction of the ω precipitates, defined by a 93at% Ti-rich iso-concentration surface, together with Mo atoms in red is shown as an inset in Fig. 1(c)[9]. The compositional partitioning of Mo across the $\beta - \omega$ interface is also shown as a proxigram analysis using ten ω precipitates, calculated with a bin size of 0.1 nm [10].

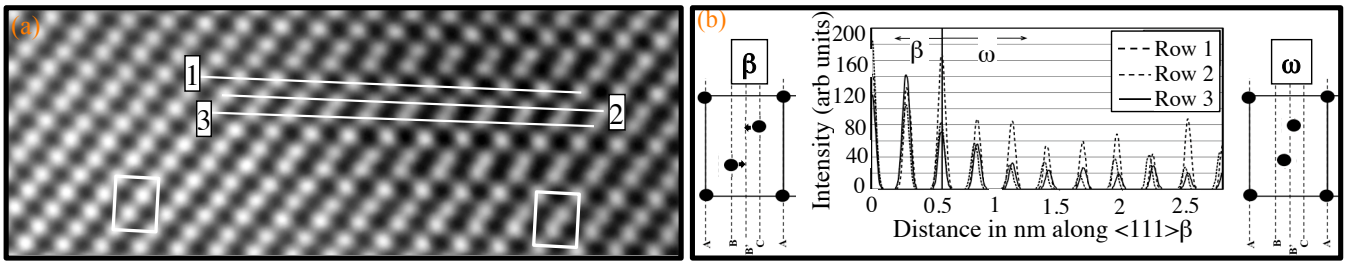

FIG. 3: (a) Enlarged HAADF-HRSTEM image of rapidly cooled Ti-9at%Mo sample showing the un-displaced and partially displaced atomic columns within the β matrix and ω embryo respectively. On (a) three consecutive $< 111 > \beta$ columns have been marked in order to calculate the atomic displacements. (b) The plot in the center shows the column intensities along rows 1, 2 and 3 (as shown in (a)) as a function of distance along the $< 111 > \beta$ directions. On both sides of the plot, cartoons show the arrangement of atoms as seen from $< 110 > \beta$ zone axis, along with the β and partially collapsed ω motifs. Small arrows show the shifts of atoms along $< 111 > \beta$ directions.

The large difference between the Mo contents of the β ($\sim$12at%) and the ω ($\sim$3.5at%) regions in this image indicates substantial rejection of Mo from the growing ω precipitates during isothermal annealing at 748K.

A filtered high-resolution HAADF-STEM image from the rapidly cooled Ti-9at%Mo sample, viewed along the $< 011 >$ direction of the β matrix is shown in Fig. 2(a). This HAADF-STEM image exhibits regions of relatively brighter and darker contrast indicative of differences in atomic masses between these regions (Z-contrast). In some cases the darker regions of lower Z exhibit shifts in the atomic columns corresponding to the nanoscale embryos of the ω–like phase. Two such ω–like embryos are marked in Fig. 2(a). Fig. 2(b) is an atom probe reconstruction depicting Ti-rich regions as an iso-concentration surface (Ti = 93 at%) together with the corresponding proximity histogram showing Mo partitioning across this interface with $\sim$ 6at% and $\sim$10at% Mo in the solute-depleted and solute-rich regions respectively [10].

Fig. 3(a) is an enlarged HAADF-HRSTEM image showing the un-displaced and partially displaced atom columns representing the β matrix and an ω–like embryo respectively. The partially collapsed {111} planes of the bcc (β) matrix are evident within the ω–like embryo in the supercell. In Fig. 3(b), we quantify the atomic displacements within the ω–like embryo with respect to the β matrix by plotting the column intensities along rows 1, 2, and 3 as a function of distance along $< 111 > \underline{e}ta$ direction. For simplicity, the origin for each row has been transposed to overlap, and the structure transitions from β to ω–like as we move from left to right along the distance axis. The spacing between adjacent atomic columns along row-1 is $3d_{222}$, where d_{222} is the interplanar spacing between the {222} planes of the β-structure. The collapse of the {111} planes can be described as a displacement wave of wavelength $\lambda = 3d_{222}$ and a corresponding wave vector of $2/3 < 111 >^{\star}$ (reciprocal space) [11, 12]. Based on this formalism, complete β to ω transformation corresponds to a longitudinal displacement wave of $0.5d_{222}$ amplitude. As seen in Fig. 3(b), the displacements of the atomic columns in rows 2 and 3 are in the range $0.16d_{222} - 0.2d_{222}$, progressively increasing on moving from left to right along the distance axis in Fig. 3(b) (from β to ω region). Consequently, the partial collapse of the {111} planes, observed here, indicates a smaller amplitude of the displacement wave compared to that seen in full collapse. This is further illustrated by crystal motifs in Fig. 3(b) depicting B and C planes forming a partially collapsed ω–like structure.

Density Functional Theory Calculations: Systems with $0at.\%$, $8.33at.\%$, and $16.66at.\%$ Mo in Ti were studied. Molybdenum atoms were added on collapsing {111} planes of β and ω titanium and these structures relaxed using Vienna Ab-initio Simulation Package (VASP) [13–15] and projector augmented wave (PAW) pseudopotentials [16]. The generalized gradient approximation of Perdew, Burke, and Ernzerhof was used [17]. A plane-wave kinetic-energy cutoff of 400 eV and 3x3x5 k-point mesh size was used to ensure an accuracy of 1 meV/atom. For titanium we treat the 3p states as valence states in addition to the usual 4s and 3d states to increase accuracy. Nudged elastic band (NEB) calculations[18] with constant cell volume yield the minimum energy pathway (MEP) for the β to ω transformation shown in Fig. 4(a). The dependence of results on system size was examined by studying systems with 12, 24, and 48 atoms in the super cell, and energy barriers are accurate to about 2 meV/atom. While there is no activation barrier for β to ω transformation in the pure Ti system, we see a local energy minimum for Ti–$8.3at.\%$ Mo system along the MEP corresponding to an average partial collapse of (222) planes. The normalized interplanar spacing for this local minimum structure is 0.25 from NEB, in agreement with experimental value of 0.20. Interestingly, $< 111 >$ atom columns with Mo atom do not collapse while a neighboring parallel $< 111 >$column with Ti does so. Such a partially collapsed structure is energetically favored over a fully collapsed structure when we have Mo atoms in the cell. For full collapse to occur, Mo atoms must diffuse out of the omega region.

We propose the following mechanism for the forma-

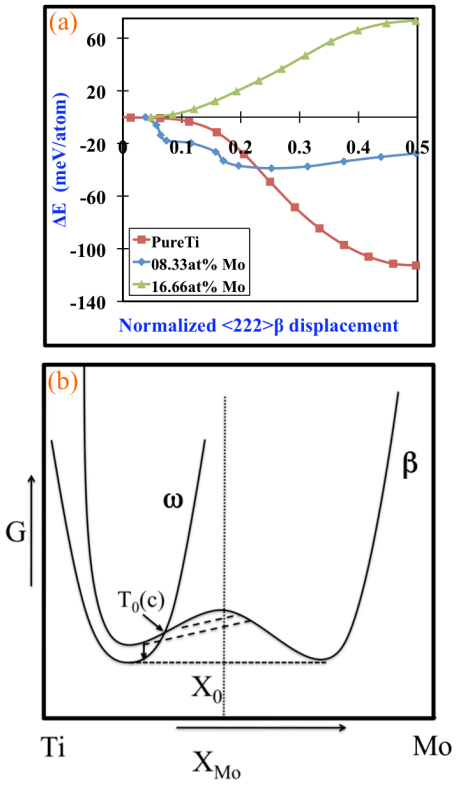

FIG. 4: (a) Nudged elastic band (NEB) results plotted for 24 atom supercell systems with 0*at.*%, 8.33*at.*%, and 16.66*at.*% Mo in Ti. ΔE is relative energy of the system along the minimum energy path with β phase taken as reference. (b) A schematic plot of Gibbs free energy versus composition.

tion of embryonic ω within the β matrix. An undercooled alloy of composition Ti-9*at.*%Mo presumably has a free energy lying within the miscibility gap (also within the spinodal) of the β phase as shown for the composition marked X_0 in Fig4(b), and consequently is unstable with respect to compositional fluctuations. This leads to nanoscale, compositional clustering (phase separation) into *Mo-enriched* and *Mo-depleted* regions, presumably by a spinodal decomposition process as indicated by the dotted lines in Fig4(b). As compositional fluctuations grow in amplitude and wavelength, the solute (Mo) depleted regions within the β phase cross the $T_0(c)$ point of intersection of the β and ω free energy curves. These solute-depleted regions now become metastable (or unstable) with respect to the structural instability causing partial collapse of the {111} β planes and the formation of ω–like embryos. Subsequent diffusional rejection of Mo from the growing embryos lead to an increase in the degree of collapse of {111} bcc planes eventually forming a fully developed hexagonal ω structure. Systematic DFT calculations to correlate local atomic displacements and composition of solute-depleted regions in Ti-Mo alloys is currently underway.

Summary: By coupling aberration-corrected HAADF-STEM with atom probe tomography and DFT calculations, the early stages of phase separation (compositional clustering) and consequent displacive collapse of {111} bcc planes within the solute-depleted regions of the β matrix of Ti-Mo alloys have been established. These results provide novel insights into the mechanisms of solid-state transformations in metallic systems by capturing the earliest stages of nucleation at atomic to near atomic spatial and compositional resolution. To the best of our knowledge, this is the first clear experimental evidence, corroborated by first principles calculations, of a close coupling between the composition and displacive component associated with product phase embryos in a first-order mixed mode transformation. We believe that this mechanism is broadly relevant to many materials.

The National Science Foundation (award# 6701956, 0700828, and 0846444) and US Air Force Research Laboratory funded this work. Experimental facilities at UNT's Center for Advanced Research and Technology and OSU's Center for the Accelerated Maturation of Materials, and the Talon Linux cluster at UNT were used.

[1] S. Banerjee & P. Mukhopadhyay, *Phase Transformations – Examples from Ti and Zr Alloys* (Pergamon, Oxford, 2007).
[2] P. D. Frost, W. M. Parris, L. L. Hirsch, J. R. Doig, & C. M. Schwartz, Trans. Amer. Soc. Metals **46**, 231243 (1954).
[3] R. R. Boyer, G. Welsch, & E. W. Collings, *Materials Properties Handbook: Ti Alloys* (ASM Handbook, 1994).
[4] I. Bakonyi, H. Ebert, & A. I. Liechtenstein, Phys. Rev. B **48**, 7841 (1993).
[5] G. B. Grad, P. Blaha, J. Luitz, & K. Schwarz, Phys. Rev. B **62**, 1274312753 (2000).
[6] D. D. Fontaine, N. E. Paton, & J. C. Williams, Acta Metall. **19**, 1153 (1971).
[7] J. C. Williams, D. D. Fontaine, & N. E. Paton, Metall. and Mater. Trans. B **4**, 27012708 (1973).
[8] M. K. Miller, K. F. Russell, K. Thompson, R. Alvis, & D. J. Larson, Micro. and Micro. **13**, 428 (2007).
[9] A. Devaraj, R. E. A. Williams, S. Nag, R. Srinivasan, H. L. Fraser, & R. Banerjee, Scripta Mater. **61**, 701 (2009).
[10] O. C. Hellman, J. A. Vandenbroucke, J. Rusing, D. Isheim, & D. N. Seidman, Micro. and Micro. **6**, 437 (2000).
[11] D. D. Fontaine, Acta Metall. **18**, 275 (1970).
[12] D. D. Fontaine & O. Buck, Philos. Mag. **27**, 967983 (1973).
[13] G. Kresse & J. Hafner, Phys. Rev. B **47**, 558 (1993).
[14] G. Kresse & J. Hafner, Phys. Rev. B **49**, 14251 (1994).
[15] G. Kresse & D. Joubert, Phys. Rev. B **59**, 1758 (1999).
[16] P. E. Blchl, Phys. Rev. B **50**, 17953 (1994).
[17] J. P. Perdew, K. Burke, & M. Ernzerhof, Phys. Rev. Lett. **78**, 1396 (1997).
[18] H. Jònsson, G. Mills, & K. Jacobsen, *Classical and Quantum Dynamics in Condensed Phase Simulations* (World Scienti c, Singapore, 1998), 1st edition.